International Journal of Thermophysics, Vol. 11, No. 5, 1990

Thermodynamic and Transport Properties of 1,2-Dichloroethane

R. Malhotra,[1] W. E. Price,[1] L. A. Woolf,[1] and A. J. Easteal[2]

Received July 24, 1989

(p, V, T) data for dichloroethane (DCE) have been obtained at 278.15, 288.15, 298.15, 313.15, 323.15, and 338.15 K for pressures either slightly below the freezing pressure or up to a maximum of 280 MPa, together with densities at 0.1 MPa. A high-pressure self-centering falling-body viscometer method has been used to measure shear viscosities at 278.15, 288.15, 298.15, 313.15, and 323.15 K for pressures either slightly below the freezing pressure or up to a maximum of 330 MPa. Self-diffusion coefficients for DCE are reported at 278.15, 288.15, 298.15, and 313.15 K for maximum pressures up to 300 MPa. Isothermal compressibilities, isobaric expansivities, and internal pressures have been evaluated from the volumetric data. The shear viscosities and self-diffusion coefficients have been interpreted in terms of a modified rough hard-spheres theory. The anomalous behavior observed for p–V–T, shear viscosities, and self-diffusion at higher temperatures and pressures is suspected to be the result of temperature and pressure altering the population ratio of the two molecular conformers, *trans* and *gauche*.

KEY WORDS: compressibility; dichloroethane; diffusion; high pressure; p, V, T, data; rough hard sphere; viscosity.

1. INTRODUCTION

1,2-Dichloroethane is of considerable interest because of the equilibrium between its molecular conformers that are related by a rotation about a single bond [1]. Both rotational isomers designated as *trans* and *gauche* coexist in the liquid phase. The various studies include temperature [2–4] and pressure effects [5, 6] on the population ratio of these molecular conformations. The system has also received substantial attention from

[1] Atomic and Molecular Physics Laboratories, Research School of Physical Sciences, The Australian National University, Canberra, A.C.T., Australia.
[2] Chemistry Department, The University of Auckland, Auckland, New Zealand.

0195-928X/90/0900-0835$06.00/0

840/11/5-1

computer simulations [7–9] since it constitutes a polar analogue to *n*-butane.

The purpose of measuring self-diffusion in dichloroethane in the dense liquid region was twofold: (a) to interpret the self-diffusion studies on the basis of a rough hard-sphere (RHS) model and (b) to investigate qualitatively the effects of the variation in the relative proportions of *trans* and *gauche* conformers with increasing temperature and pressure. Shear viscosities were measured to complement the self-diffusion measurements. Accurate high-pressure volumetric data were also determined, as they were necessary for the diffusion and shear viscosity measurements and to test the RHS model.

2. EXPERIMENTAL

The 1,2-dichloroethane (DCE) was UNIVAR AnalaR-grade material of stated purity minimum 99.0 mol%, which was used without further purification except for storage over molecular sieves for several weeks before use to remove water and other low molecular weight impurities.

2.1. Volumetric Measurements

Volume ratios, k, defined by

$$k = V_p/V_{0.1} \tag{1}$$

where $V_{0.1}$ and V_p are volumes of a fixed mass of liquid at 0.1 MPa and pressure p, respectively, and were determined using a bellows volumometer described previously [10, 11]. The measurements were made at 278.15, 288.15, 298.15, 313.15, 323.15, and 338.15 K. The pressure range for these measurements is from about 2.5 MPa to either about 280 MPa or a lower pressure slightly below the freezing pressure [12] at the temperature of measurement. The estimated uncertainty in the measured volume ratios correspond to about ± 0.02–0.04% in density at pressures above 50 MPa, increasing to $\pm 0.1\%$ at pressures approaching 0.1 MPa.

Densities of DCE were measured at 0.1 MPa, using an Anton Paar Model DMA 602 densimeter, for temperatures of 278.15, 298.15, 323.15, and 338.15 K with an uncertainty of $\pm 0.003\%$.

2.2. Viscosity Measurements

A high-pressure falling-body viscometer was constructed, similar in most details to that of Dymond et al. [13]. This instrument enables shear viscosities to be determined from measurements of the terminal velocity of

a self-centering sinker falling axially down the center of a vertical circular tube containing the liquid. The sinker and tube were constructed from the same nonmagnetic 316 stainless steel. A section through the viscometer is illustrated in Fig. 1. The viscometer tube, with an external diameter of 13 mm, is 190 mm in length. The tube bore was 6.5 ± 0.005 mm, with a surface finish of 0.15 μm. The sinker was 14 mm long and 6.3 mm in diameter, with a surface finish of 0.5 μm; a small ferrite core was embedded into the sinker.

The position of the sinker was detected by the change in inductance it causes as it passed through a pair of coils, situated 100 mm apart, wound on the outside of the viscometer tube. Each coil was wound from approximately 65 turns of 0.16-mm insulated copper wire and the ends soldered to pin connections attached to the end plug of the viscometer. The coils formed two active arms of an AC bridge with the other two arms remote from the viscometer. The passage of the ferrite core through each coil in turn resulted in an imbalance of the electrical signal which was amplified and used to gate a timer. The timer was triggered on and off at

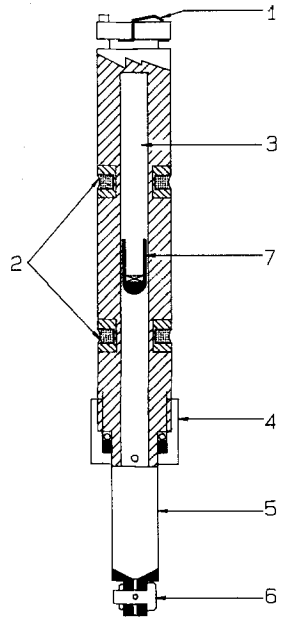

Fig. 1. The high-pressure viscometer: 1, pin connection; 2, coils; 3, viscometer bore; 4, end plug; 5, PTFE bellows; 6, valve; 7, sinker.

the onset of the first and the second out-of-balance signals, respectively. The input level, at which the trigger operated the timer, was offset to a threshold to avoid false triggering caused by background noise in the circuit. Three or more consecutive readings of the falltime of the sinker falling concentrically in the tube were taken to obtain the mean fall time with a maximum uncertainty of $\pm 0.1\,\%$.

The pressure was transmitted to the liquid in the viscometer tube via a collapsible thin-walled (0.25-mm) PTFE bellows, similar to one described earlier [14] but with a valve at the end. The valve enabled the fluid in the viscometer to be freed of trapped gases and adjustment of the liquid volume to cover the full temperature range of the measurements. The pressure vessel, constructed of IMI titanium 318 alloy, was held halfway along its length in a housing which was connected to the shaft of an AC/DC stepping motor installed outside the bath. The computer-controlled stepping motor rotates the pressure vessel through 180° in a clockwise or anticlockwise direction to position the sinker above the first measuring coil. The pressure was measured using a Heise-Bourdon gauge, 0–400 MPa, calibrated with a deadweight gauge with an overall accuracy of $\pm 0.1\,\%$.

The pressure vessel was immersed in a closed bath containing oil. The temperature of the bath was controlled to ± 0.005 K at each temperature and measured with an accuracy of ± 0.01 K with a calibrated platinum resistance thermometer.

For laminar flow in the viscometer, the viscosity coefficient, η_p, at pressure p and temperature T is related to the sinker fall time, t_p, by the equation [15]

$$\eta_p = \frac{t_p(1-\rho_L/\rho_s)}{A[1+2\alpha_s(T-T_r)][1-2\beta(p-p_0)]} \tag{2}$$

where ρ_L and ρ_s are, respectively, the liquid and sinker densities at T and p, A is the viscometer constant, α_s is the linear expansion coefficient ($1.6\times10^{-5}\,K^{-1}$), β is the linear compressibility of the sinker and tube ($2.0\times10^{-12}\,Pa^{-1}$), T_r is the reference temperature (298.15 K), and p_0 is the atmospheric pressure. The viscometer constant, A, was determined by calibration with hexane, dodecane, bromocyclohexane, water, toluene, heptane, and Cannon Instrument Company oils S3 and S6 at atmospheric pressure at 298.15 K. For the sinker used in this work, having density ρ_s ($=7285\,kg\cdot m^{-3}$), the viscometer constant, A, has a linear relationship with the quantity $t(1-\rho_L/\rho_s)$

$$A = A_r + B_r[t(1-\rho_L/\rho_s)] \tag{3}$$

where A_r and B_r are least-squares fitted parameters, having values 28500.5 and 0.304464, respectively, ρ_L is the atmospheric pressure density of the calibration fluids, and t is the time taken for the sinker to pass through the pair of coils. To minimize systematic errors the viscometer is used to determine the viscosity ratio, η_p/η_0, given by

$$\frac{\eta_p}{\eta_0} = \frac{t_p}{t_0} \cdot \frac{(1-\rho_L/\rho_s)}{(1-\rho_{L0}/\rho_{s0})} \cdot \frac{[1+(B_r/A_r)\, t_0(1-\rho_{L0}/\rho_{s0})]}{[1+(B_r/A_r)\, t_p(1-\rho_L/\rho_s)]} \cdot \frac{1}{1-2\beta(p-p_0)} \tag{4}$$

where ρ_{L0} and ρ_{s0} are the liquid and sinker densities at atmospheric pressure, and the subscript 0 indicates a value at atmospheric pressure. The sinker density at atmospheric pressure and pressure p for temperature T is given by

$$\rho_{s0} = \rho_{298.15,0.1}/[1+3\alpha_s(T-298.15)] \tag{5}$$

$$\rho_s = \rho_{s0}/[1-3\beta(p-p_0)] \tag{6}$$

The accuracy of the experimental viscosity ratio is estimated to be $\pm 2\%$.

Viscosities of DCE were measured at 0.1 MPa, with an uncertainty of $\pm 0.5\%$, using a flared capillary viscometer for temperatures 298.15, 313.15, and 323.15 K. Atmospheric pressure viscosities at other temperatures were obtained from correlation of the available literature values (Section 3.3).

2.3. Self-Diffusion Coefficients

Measurements of the self-diffusion coefficient, D, were made using carbon-14-labeled, 1,2-dichloroethane as tracer. The labeled material, from the Radiochemical Centre, Amersham, was used without further purification; counting procedures were standard [16]. A high ratio of active/background counts was obtained by using approximately 0.74 MBq of tracer for each experiment. At atmospheric pressure the conventional diaphragm-cell method [16] was used; recent modifications to the cell and associated equipment have been described [17]. For higher pressures, the high-pressure diaphragm-cell technique [18, 19] was used, with an exception for the self-diffusion coefficients measurements at 298.15 K, for which the NMR method was used as described in detail elsewhere [19, 20]. The accuracy of the experimental values of D is believed to be ± 0.5 to $\pm 1\%$ at 0.1 MPa and $\pm 2\%$ at the higher pressures.

3. RESULTS AND DISCUSSION

3.1. Volumetric Data

Experimental values for the density at 0.1 MPa, together with literature data [21–24], are given in Table I. The combined data are represented by a third-degree polynomial in temperature (T)

$$\rho = -0.86457 + 1.49656 \times 10^3/T - 3.68056 \times 10^5/T^2 + 3.263 \times 10^7/T^3 \quad (7)$$

(ρ in g · cm^{-3}; T in K) with rms deviation of the experimental points from the calculated curve 1.32×10^{-4}).

Experimentally determined volume ratios, k, were expressed as the secant bulk modulus, K, defined by

$$K = p/(1-k) \quad (8)$$

and fitted to cubic equations of the form

$$K = \sum_{i=0}^{3} A_i p^i \quad (9)$$

The coefficients of Eq. (9) are listed in Table II. The maximum deviation between the calculated and the experimental volume ratios is 0.012%. The present volume ratio values agree within ±0.2% with those of Kumagai and Takahashi [22] at 298.15 and 323.15 K and Newitt and Weale [25] at 298.15 K.

Equation (9), though a very good representation of the pressure dependence of the experimental volume ratios at constant temperature, cannot be extrapolated accurately to pressures which substantially exceed

Table I. Densities at 0.1 MPa

	ρ (kg · m^{-3})	
T (K)	This work	Literature
278.15	1274.89	
298.15	1245.98	1245.80 [21]
		1246.00 [23]
		1246.30 [22]
		1245.30 [24]
323.15	1208.91	1209.48 [22]
338.15	1186.31	

Table II. Coefficients of Eq. (9) for Secant Bulk Modulus

R (K)	A_0 (MPa)	A_1	$-A_2$ (GPa^{-1})	A_3 (GPa^{-2})	100 ($\delta k/k$)
278.15	1381.831	6.608097	19.251343	48.033	0.012
288.15	1310.476	5.492829	7.568392	11.300	0.004
298.15	1230.131	4.985762	4.138318	4.373	0.004
313.15	1089.992	4.804205	4.016597	3.925	0.003
323.15	1025.126	4.374219	1.647144	−0.736	0.009
338.15	894.248	5.052601	5.974820	7.350	0.004

the highest experimental pressure. Also, the coefficients cannot be used to calculate reliably the densities at extrapolated temperatures. The volume ratios were fitted therefore to the modified Tait equation [26] expressed here as

$$1 - k = C \log[(B + p)/(B + p_0)] \tag{10}$$

where p_0 is the reference pressure, usually 0.1 MPa, p is the working pressure, and the constants B and C are adjustable parameters. The coefficients B and C of Eq. (10) are given in Table III; this equation does not fit volume ratio data quite as well as Eq. (9) but has the advantage of being reliable for extrapolation of volume ratios to pressures beyond the experimental pressure range. It may also be used to represent accurately the effect of temperature by using C as a constant independent of temperature for a given substance, while the parameter B is expressed as a function of temperature [27, 28]. Kumagai and Takahashi [22] made $C =$

Table III. Optimized Tait Coefficients Eq. (10) and Comparison of Calculated $V_p/V_{0.1}$ from Eqs. (10) and (11) with the Measured $V_p/V_{0.1}$

T (K)	B (MPa)	C	$100(\delta k/k)^a$	$100(\delta k/k)^b$
278.15	134.8	0.2194	0.011	0.03
288.15	127.8	0.2226	0.011	0.01
298.15	116.0	0.2193	0.010	0.05
313.15	106.2	0.2265	0.010	0.04
323.15	99.4	0.2288	0.012	0.06
338.15	86.8	0.2236	0.016	0.04

[a] The average percentage deviation of calculated $V_p/V_{0.1}$, using optimized B and C from columns 2 and 3, respectively, from the measured $V_p/V_{0.1}$.

[b] The average percentage deviation of calculated $V_p/V_{0.1}$ from the measured $V_p/V_{0.1}$, using $C = 0.22$ and B from Eq. (11).

0.2325 for DCE and tabulated corresponding B values for the isotherms at 298.15, 323.15, and 348.15 K up to a maximum pressure of 101.3 MPa. Newitt and Weale [25] obtained $C = 0.2233$ for their only isotherm, up to 101.3 MPa at 298.15 K. The present measurements can be reproduced using $C = 0.22$, with B represented as a function of temperature by

$$B = 791.812 - 3.5827T + 0.00441T^2 \tag{11}$$

(B in MPa, T in K) with root mean square deviation of the B values from the calculated values of 0.88%.

In Table III, the accuracy of volume ratios calculated from the Tait equation with C fixed at 0.22 and B given by Eq. (11) is compared with the accuracy of volume ratios calculated from the optimized B and C values. The maximum deviation of the calculated volume ratio from the measured value was 0.14% for the measurement at the highest pressure (281 MPa) at 323.15 K, while at the other temperatures, the maximum deviation of the calculated from the experimental value was always less than 0.10%, anywhere in the pressure range 0.1 to 280 MPa.

It has been found that extrapolation of B expressed as a function of reduced temperature for normal alkanes [29] (or B as a function of temperature for fluid toluene [30]) is a reasonable means of predicting densities at temperatures either up to the normal boiling point or 0.64 times the critical temperature, whichever is the smaller. Equation (11) was extrapolated by 10 K to obtain a value of B for DCE at 348.15 K; the predicted values of the volume ratios were within 0.03% of the measured values [22] at 348.15 K, while at 373.15 K, 17 K above the normal boiling point of DCE and 35 K above our highest experimental temperature, the predicted volume ratios differed by about 0.3% from the experimental ones [22].

Isothermal compressibilities, κ_T, were calculated from the coefficients of Eq. (9) at each temperature by using the relationship [31]

$$\kappa_T = -[1/(p-K)][1-(p/K)(\partial K/\partial p)_T] \tag{12}$$

Isobaric expansivities, α, were calculated using the densities at 0.1 MPa, given by Eq. (7), and volume ratios from Eq. (9), using coefficients given in Table II, and then evaluating the molar volume (V_m) as a function of temperature at 10, 20, 50, 100, 150, 200, 250, and 275 MPa, fitting V_m to a quadratic in T, and utilizing the relationship

$$\alpha = (1/V_m)(\partial V_m/\partial T)_p \tag{13}$$

The expansivities and compressibilities are listed in Table IV. The probable uncertainties in κ_T and α are ± 1–2 and ± 2–3%, respectively, for

Table IV. Isobaric Expansivities (α, in K^{-1}) and Isothermal Compressibilities (κ_T, in MPa^{-1})

		p (MPa)							
T (K)	Property	0.1	10	20	50	100	150	200	250
278.15	$10^3\alpha$	1.12	1.09	1.04	0.91	0.76	0.67		
	$10^4\kappa_T$	7.23	6.66	6.20	5.24	4.33	3.63	2.82	
288.15	$10^3\alpha$	1.14	1.10	1.06	0.92	0.77	0.68	0.51	
	$10^4\kappa_T$	7.63	7.09	6.63	5.58	4.48	3.79	3.27	2.80
298.15	$10^3\alpha$	1.17	1.12	1.07	0.93	0.79	0.70	0.56	
	$10^4\kappa_T$	8.12	7.57	7.09	5.94	4.69	3.89	3.33	2.90
313.15	$10^3\alpha$	1.21	1.14	1.08	0.95	0.81	0.72	0.63	
	$10^4\kappa_T$	9.17	8.50	7.91	6.55	5.10	4.20	3.59	3.13
323.15	$10^3\alpha$	1.23	1.15	1.09	0.96	0.82	0.73	0.68	
	$10^4\kappa_T$	9.75	9.06	8.45	6.98	5.36	4.36	3.70	3.27
338.15	$10^3\alpha$	1.26	1.17	1.11	0.97	0.84	0.75	0.75	
	$10^4\kappa_T$	11.17	10.14	9.28	7.40	5.59	4.56	3.86	3.32

pressures higher than 50 MPa, provided the experimental pressure range for volume-ratio measurements exceeds 150 MPa. At atmospheric pressure the thermal expansivities are in good agreement with the literature values: 298.15 K, 1.17×10^{-3} (this work) and $1.18 \times 10^{-3}\ K^{-1}$ [32]; at 313.15 K, 1.21×10^{-3} and $1.23 \times 10^{-3}\ K^{-1}$ [33] and $1.19 \times 10^{-3}\ K^{-1}$ [36]; and 323.15 K, 1.23×10^{-3} and $1.22 \times 10^{-3}\ K^{-1}$ [36].

The compressibilities at atmospheric pressure for temperatures, 278.15 to 338.15 K, can be represented (standard deviation, 7.2×10^{-2}) as a function of temperature by

$$\kappa_T = 35.481 - 0.2389(T) + 4.9366 \times 10^{-4}(T)^2 \qquad (14)$$

where κ_T is in $10^4\ MPa^{-1}$ and T is in K.

Figure 2 compares the smooth curve obtained from Eq. (14) with the literature isothermal compressibilities [32–36] at atmospheric pressure. The literature values agree with those from Eq. (14) within ± 1–2%; in particular, the agreement with the Staveley data [36] is better than ± 0.5%. Also, the equation can be extrapolated at either end of the experimental range to compare the isothermal compressibilities with literature values: at 273.15 K, 7.06×10^{-4} [Eq. (14)] and $6.91 \times 10^{-4}\ MPa^{-1}$ [35]; at 343.15 K, 11.63×10^{-4} and $11.76 \times 10^{-4}\ MPa^{-1}$ [35]; and at 353.15 K, 12.68×10^{-4} and $12.79 \times 10^{-4}\ MPa^{-1}$ [35].

The plot of compressibility against molar volume is shown in Fig. 3. The compressibilities for all temperatures except 338.15 K are close to the

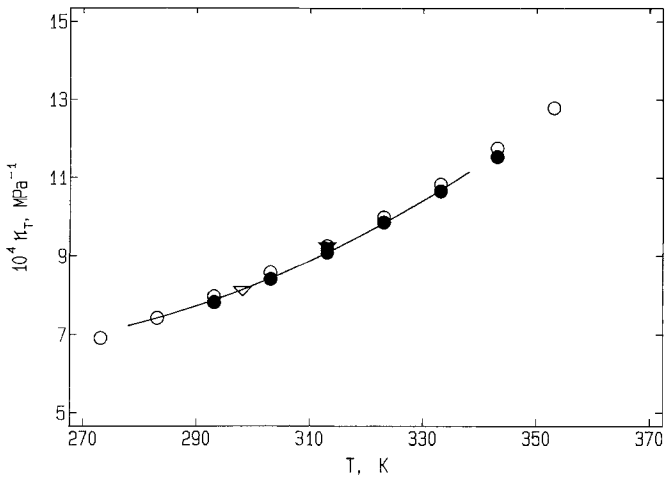

Fig. 2. Comparison of atmospheric pressure isothermal compressibilities [Eq. (14)] with the literature values. ——, Eq. (14); ▽, Ref. 32; ▼, Ref. 33; ■, Ref. 34; ●, Ref. 35; ○, Ref. 36. Note that at 303 K values of Refs. 34–36, and at 313 K values of Refs. 33, 35, and 36, are close to coincidence.

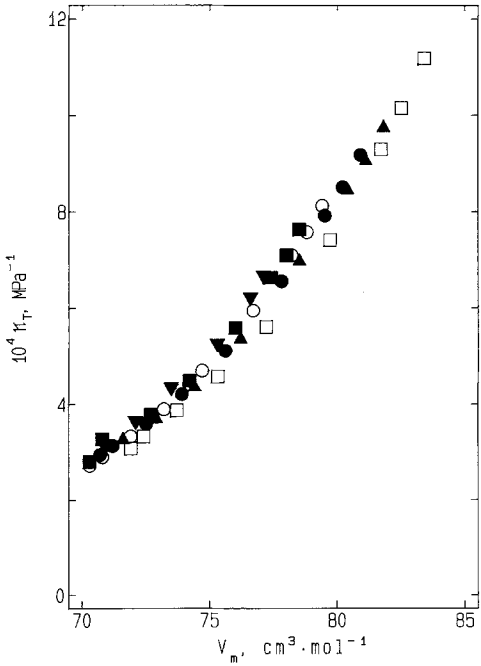

Fig. 3. Isothermal compressibility as a function of molar volume at various temperatures. ▼, 278 K; ■, 288 K; ○, 298 K; ●, 313 K; ▲, 323 K; □, 338 K.

same curve, although there is an overall slow decrease in κ_T with increasing temperature at constant volume.

Compressibilities can also be calculated from Eq. (10) using the relationship [31]

$$\kappa_T = -(1/k)(\partial k/\partial p)_T \tag{15}$$

so that the isothermal compressibility κ_T is expressed as

$$\kappa_T = \frac{1}{2.3026\,k} \cdot \frac{C}{(B+p)} \tag{16}$$

where $C = 0.22$ for DCE, k is calculated using Eq. (10), and B, for temperature T, is calculated using Eq. (11). Values of κ_T calculated from Eq. (16) have a maximum deviation, from the corresponding compressibilities in Table IV, of less than 1.4% with the exception of values for pressures above 250 MPa at 338.15 K, where the deviations exceed 3%. However, it should be reasonable to use Eq. (16) to calculate isothermal compressibilities with a probable uncertainty of 1–2% in the temperature range 278.15 to 348.15 K for pressures up to 275 MPa.

The isothermal energy coefficient or internal pressure p_{int} is related to the thermal pressure coefficient $(\partial p/\partial T)_v$, by

$$p_{\text{int}} = (\partial U/\partial V)_T = T(\partial p/\partial T)_v - p \tag{17}$$

where U is the internal energy. The values of p corresponding to selected values of V_m were determined at each temperature by interpolation of cubic spline fits of 10 values of p against V_m, at each temperature. The thermal pressure coefficients $(\partial p/\partial T)_v$ were calculated from quadratic fits of these values of p against T. The values of p_{int} are listed in Table V; they are estimated to have a probable uncertainty of the order of $\pm 3\%$.

The volume dependence of the internal pressure for DCE, at constant temperature, shown in Fig. 4, is unusual. The curves for internal pressure p_{int} versus V_m for all temperatures, except 338.15 K, are essentially those of a typical nonassociated liquid [37]. The internal pressure decreases with increasing temperature at large constant volumes as expected for normal behavior of liquids [38], and $(\partial p_{\text{int}}/\partial T)_v$ changes sign at about 75 $\text{cm}^3 \cdot \text{mol}^{-1}$. However, p_{int} increases with increasing volume at constant temperature (except at 338.15 K), contrary to normal behavior as exemplified by carbon tetrachloride [38]. Short-range intermolecular interactions evidently become significant when interparticle distances are sufficiently reduced by the application of pressure.

Table V. Internal Pressure (p_{int}, in MPa)

	T(K)					
V_m ($cm^3 \cdot mol^{-1}$)	278.15	288.15	298.15	313.15	323.15	338.15
72	332	340	350	373	388	403
73	362	366	373	388	397	406
74	386	387	390	398	403	407
75	404	402	403	406	407	406
76	417	414	413	411	410	406
77	427	422	419	414	411	404

3.2. Self-Diffusion Coefficients

The experimental results are given in Table VI. They are fitted within the experimental accuracy of ±2% by

$$\ln(D) = A_1 + A_2(p) + A_3(p)^2 \tag{18}$$

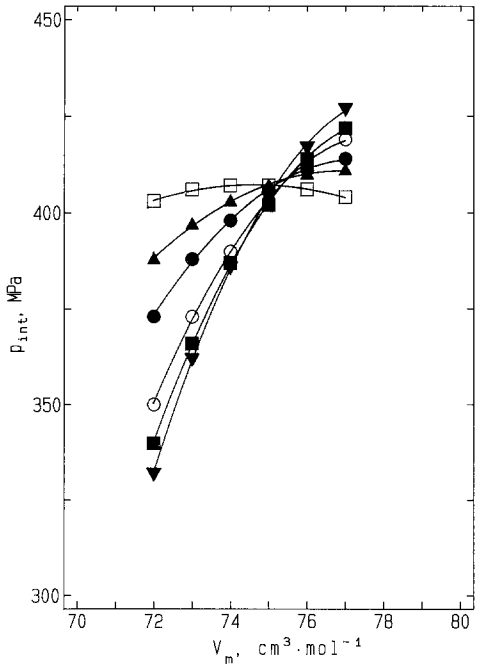

Fig. 4. Volume and temperature dependence of the internal pressure. Symbols as in the legend to Fig. 3.

Table VI. Self-Diffusion Coefficients

T (K)	p (MPa)	10^9 ($m^2 \cdot s^{-1}$)	T (K)	p (MPa)	10^9 ($m^2 \cdot s^{-1}$)
278.15	0.1	1.184	288.15	0.1	1.460
	40.0	0.967		58.3	1.098
	80.7	0.795		99.5	0.892
	135.2	0.604		132.3	0.756
				225.6	0.507
298.15	0.1	1.692			
	16.6	1.521	313.15	0.1	2.110
	49.4	1.298		34.3	1.590
	100.8	0.985		37.6	1.626
	150.0	0.793		67.4	1.363
	201.4	0.652		130.7	0.947
	240.3	0.566		283.0	0.650
	279.5	0.490			

where D is in $10^{-9}\ m^2 \cdot s^{-1}$ and p is in MPa. The values of the coefficients A_1, A_2, and A_3 are given in Table VII.

Rough hard-sphere (RHS) theory [39] has been widely used to interpret self-diffusion coefficients [40–45]. For a liquid which behaves as a smooth hard-sphere fluid the Enskog dilute fluid self-diffusion coefficient at low densities is defined by [46]

$$(nD)_0 = (3/8)(RT/\pi M)^{1/2}\sigma^{-2} \tag{19}$$

where T is the Kelvin temperature, M the molar mass, σ the hard-sphere diameter, and n the number density. Chandler [39] considered the coupling of translational and rotational motion during collisions between molecules and related the diffusion coefficients for the rough and smooth hard-sphere models by the introduction of a coupling factor A_D

$$D = A_D D_{SHS} \tag{20}$$

where $0 < A_D < 1$ was considered to be rigorously independent of density.

Table VII. Coefficients of Eq. (18) for Self-Diffusion Coefficient

Temperature (K)	A_1	$10^3 A_2$	$10^7 A_3$	rms % dev
278.15	−20.55507	−4.956	−0.848435	0.013
288.15	−20.34258	−5.274	25.2817	0.022
298.15	−20.20821	−5.688	47.5415	0.043
313.15	−19.96756	−7.714	124.185	0.059

Alder, Gass, and Wainwright (AGW) [47], on the basis of MD calculations, determined the dependence of the ratio D_{SHS}/D_E (where D_E is the Enskog dense fluid diffusion coefficient) on number density. More extensive simulations, designed to cover the experimentally accessible liquid density range, led to the relation [48]

$$D_{SHS} = (nD)_0(1.02732 - 0.91497\rho^* - 0.07427\rho^{*2}) \qquad (0.35 \leqslant \rho^* \leqslant 0.94) \tag{21}$$

where ρ^* is the reduced density equal to $n\sigma^3$ in the specified range. Speedy [49] recently made an extensive literature survey of MD simulation data for hard-sphere fluids and proposed as an alternative to Eq. (21) the expression

$$D_{SHS} = (nD)_0(1 - \rho^*/1.09)[1 - \rho^{*2}(0.4 - 0.83\rho^{*2})] \tag{22}$$

which was claimed to be more accurate at high densities. Recently, for typical liquid densities ($\rho^* \geqslant 0.7$), Meckl and Zeidler [45] have replaced Eq. (21) with a simpler expression

$$D_{SHS} = (nD)_0(1.07766 - 1.03772\rho^*) \qquad (0.7 \leqslant \rho^* \leqslant 0.94) \tag{23}$$

Substitution of $(nD)_0$ [Eq. (19)] and inclusion of the coupling factor (Eq. 20) into Eq. (23) yield

$$D = \tfrac{3}{8}A_D(RT/\pi M)^{1/2}[1.07766(V_m/L\sigma^2) - 1.03772\sigma) \tag{24}$$

with V_m the molar volume, and L the Avogadro constant.

Accordingly, a linear relation is expected from plots of the diffusion coefficient D against the molar volume V_m, shown in Fig. 5. However, the predicted linear variation occurs for DCE only at 278.15 and 288.15 K. From the least-squares fitted values of slope and intercept, assuming the linear relationship, the parameters σ and A_D are extracted for those temperatures, and the σ values are reported in Table VIII.

Speedy [49] also proposed

$$nD_{SHS}/(nD)_0 = 1 - \rho^*/1.09 \tag{25}$$

based on the existence of a singularity for the hard-sphere fluid at a reduced density $\rho^* = 1.09$ at which diffusion ceases because the hard-sphere fluid becomes incompressible and unstable [50, 51]; this idea is supported by calculations [52, 53] which locate a glass transition at the same ρ^*. Once again, the expected linear relationship between D and ρ^* is obeyed by DCE only at 278.15 and 288.15 K. The values of σ for these

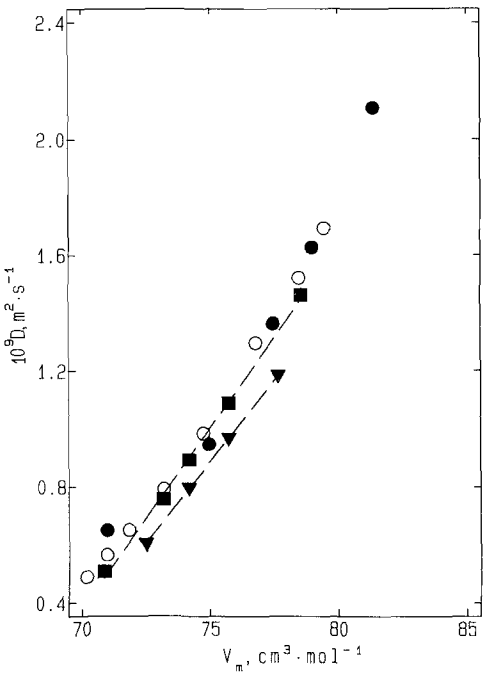

Fig. 5. Diffusion coefficient as a function of molar volume at temperatures of measurement. ▼, 278 K; ●, 288 K; ○, 298 K; ●, 313 K.

Table VIII. Equivalent Hard-Sphere Diameters for DCE

				nm		
T (K)	p_f[a] (MPa)	$V_p/V_{0.1}$	V_{fp}[b] ($cm^3 \cdot mol^{-1}$)	σ Eq. (26)	σ [49], Eq. (25)	σ [45], Eq. (24)
278.15	205.9	0.9118	70.78	0.480_3	0.497_0	0.487_3
288.15	262.6	0.8922	70.07	0.478_9	0.496_4	0.486_3
298.15	320.7	0.8739	69.42	0.477_2	—	—
313.15	410.2	0.8445	68.71	0.476_7		
323.15	471.4	0.8263	67.60	0.473_0		
338.15	556.0	0.8055	67.10	0.471_8		

[a] p_f, freezing pressure.
[b] V^{fp}, molar volume at freezing pressure.

temperatures reported in Table VIII were calculated by optimizing the value of σ which satisfy the condition that $D \to 0$ as $\rho^* \to 1.09$.

Easteal and Wollf [54] obtained σ from the density of the experimental fluid at its freezing pressure by assuming that the fluid acts as a smooth hard-sphere fluid for which

$$\sigma = 0.11611\ V_{fp}^{1/3} \tag{26}$$

where σ is in nm and V_{fp} is in $cm^3 \cdot mol^{-1}$. The pressure for DCE at each temperature for which volume ratios were measured was obtained from the compilation by Babb [12] for temperatures up to 323.15 K and at 338.15 K by extrapolation. Values of $V_p/V_{0.1}$ at the freezing pressure at each temperature were then calculated using Eq. (10) in conjunction with molar volumes at 0.1 MPa from Eq. (7) to calculate the molar volume V_{fp} at the freezing pressure for each temperature. The values of σ are given in Table VIII together with the data used for the calculations. The temperature variation of σ ($278\ K \leqslant T \leqslant 338\ K$) can be expressed by

$$\sigma = 0.5415 - 2.823 \times 10^{-4}(T) + 2.23 \times 10^{-7}(T)^2 \tag{27}$$

where σ is in nm and T is in K. It is notable that even though estimation of $V_p/V_{0.1}$ at the freezing pressures above 298 K involves a lengthy extrapolation of Eq. (10), the estimated values of σ form a smooth curve with the values for the lower temperatures and the maximum deviation of the estimated σ from the curve given by Eq. (27) is 0.13% at 323.15 K. The comparison of σ values, obtained by these three approaches in Table VIII, suggests that obtaining σ from the freezing pressure is most appropriate in this case, as σ has a smooth variation with temperature in the expected direction [39] for all temperatures.

The values of A_D obtained using σ from Eq. (27) and D_{SHS} from Eq. (22) with Eq. (20) are shown as a function of packing fraction Z ($=\pi\rho^*/6$) in Fig. 6. A strong density dependence of A_D for DCE at 298.15 K was observed earlier [41] in this laboratory; the present values at other temperatures (278–313 K) show that A_D decreases with increasing temperature at constant packing fraction and decreases with increasing packing fraction at constant temperature. Such behavior has been found previously only in the case of benzene [41], for which temperature dependent variations in packing geometry were proposed to account for the large changes in A_D with density and temperature.

Dymond [55] defined a temperature-independent reduced diffusion coefficient

$$D^* = [nD/(nD)_0](V_m/V_0)^{2/3} \tag{28}$$

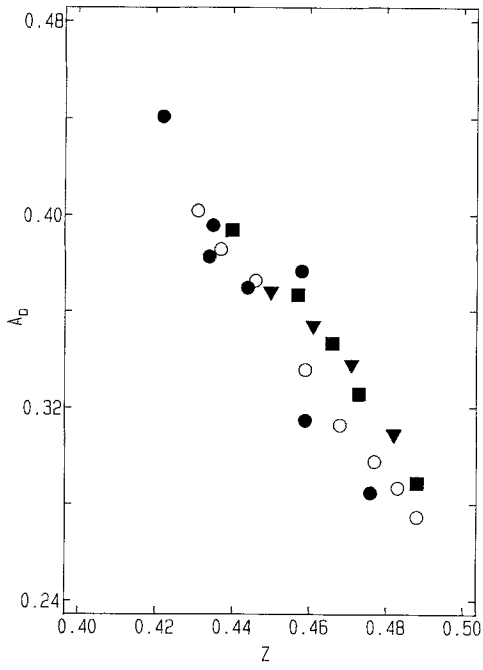

Fig. 6. Dependence of A_D factors for diffusion on packing fraction. Symbols as in the legend to Fig. 5.

where n is the number density corresponding to the experimental diffusion coefficient D, V_0 is the close-packed volume of hard spheres, and $(nD)_0$ is the Enskog dilute fluid diffusion coefficient defined by Eq. (19). In terms of experimental quantities

$$D^* = 1.744 \times 10^6 D V_m^{-1/3} (M/T)^{1/2} \tag{29}$$

Dymond [55] suggested that D^* should depend only on V_m/V_0. To obtain $V_0 = L\sigma^3/\sqrt{2}$ we used the values of the temperature-dependent core size σ from Eq. (27). In practice, a fit of D^* against V_m/V_0 should be within the experimental uncertainty of the measured self-diffusion coefficients of the liquid as evidence that the correlation treatment is insensitive to the shape of the molecule [56]. D^* for dichloroethane are plotted against V_m/V_0 $(=\sqrt{2}/n\sigma^3)$ in Fig. 7. The close coincidence of the D^* about the same curve illustrates the consistency of our method of obtaining σ from the molar volumes of the fluid at the freezing pressure. Over the four isotherms (278–313 K) included in the fit D^* can be represented within 6% by one curve given by the equation

$$D^* = 0.949_8 - 1.516_2(V_m/V_0) + 0.603_9(V_m/V_0)^2 \tag{30}$$

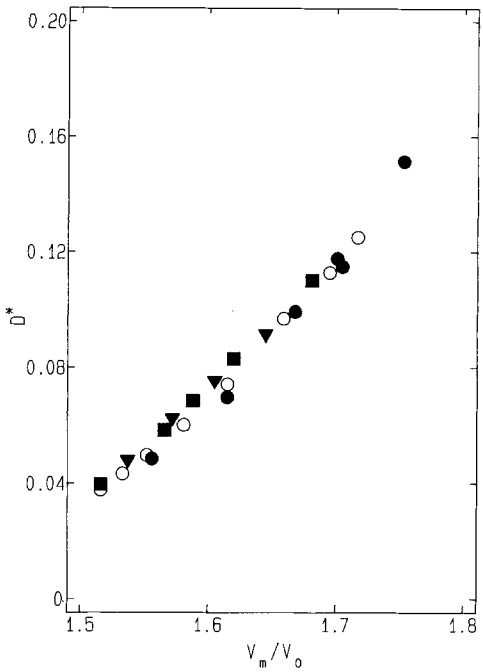

Fig. 7. Variation of reduced diffusion coefficient D^* with density (V_m/V_0) at various temperatures. Symbols as in the legend to Fig. 5.

with the exception of two points [D^* deviating from Eq. (30) by 9 and 8% for pressures 131 and 283 MPa, respectively] at 313.15 K.

3.3. Shear Viscosity

3.3.1. At 0.1 MPa. The present experimental values for the viscosity, η, at 0.1 MPa, together with literature data [21, 57–59] are given in Table IX. Discrepancies of up to $\pm 2\%$ occur in the literature values where data exist at the same temperature, for instance, the reported values for the viscosity at 298.15 K (Table IX).

The viscosity, at 0.1 MPa, for DCE can be obtained from the Bingham viscosity–temperature relationship [21]

$$T = 0.44121/\eta + 2219.3 - 258.83\eta \tag{31}$$

Reid *et al.* [57] have suggested the following viscosity–temperature

Table IX. Shear Viscosity at 0.1 MPa

	η (mPa · s)	
Temperature (K)	This work	Literature
298.15	0.777	0.773 [59] 0.787 [60] 0.783 [61]
313.15	0.647	0.644 [57]
323.15	0.585	

relationship, for DCE at 0.1 MPa, for temperatures in the range from 273.15 to 373.15 K:

$$\ln \eta = -3.926 + 1091/T \tag{32}$$

The viscosities calculated using Eq. (31) agree within 1% with the experimental data for the temperature range 288 to 303 K, but the calculated viscosities may not be reliable as the temperature range for the validity of the equation is uncertain. Equation (32) fits the experimental values within better than ±2% with an exception of the deviation from the experimental value at 273.15 K of 4%.

3.3.2. High-Pressure Viscosities. Measurements of fall times were made for DCE at pressures up to near the freezing pressure or 330 MPa for temperatures up to 323.15 K. The ratios of viscosity at pressure η_p to viscosity at atmospheric pressure $\eta_{0,1}$, calculated from Eq. (4), are presented in Table X, together with values for the densities under the corresponding conditions calculated from the volume ratio using Eq. (10) and atmospheric pressure densities from Eq. (7).

Dymond and Brawn [62] proposed a free volume equation of the form

$$\ln \eta' = A_f + B_f V_f/(V_m - V_f) \tag{33}$$

where η' is the reduced viscosity defined as

$$\eta' = 100\eta V_m^{(2/3)}/(MT)^{0.5} \tag{34}$$

and has units of mP · s, V_m is in $cm^3 \cdot mol^{-1}$, and M is the molar mass in 10^{-3} kg · mol^{-1}; the coefficients A_f, B_f, and V_f are adjustable parameters obtained from the experimental viscosities by the least squares method; A_f and B_f are used to allow for the effects of nonspherical molecular shape

and of translation-rotational coupling. Equation (33) has been used to represent satisfactorily the viscosity data for pure components and their mixtures [63–65] using A_f equal to -1. The optimized values of the coefficients B_f and V_m for DCE are listed in Table XI, in which the root mean square percentage deviations are also shown. As expected, for real molecules, the characteristic volume V_f decreases as the temperature increases with the exception of V_f at 323.15 K. (However, V_f is not close to V_0, which is the volume of close-packed hard spheres.)

Table X. Shear Viscosity Ratios for DCE

Temperature (K)	Pressure (MPa)	Density ($kg \cdot m^{-3}$)	$\eta_p/\eta_{0.1}$
278.15	0.1	1274.89	1.000
	44.6	1310.47	1.332
	85.0	1336.85	1.702
	132.3	1363.75	2.313
288.15	0.1	1260.00	1.000
	48.5	1300.42	1.348
	92.7	1329.90	1.743
	148.8	1361.42	2.322
	188.2	1380.78	2.813
	233.8	1400.84	3.621
298.15	0.1	1245.70	1.000
	39.5	1281.32	1.291
	67.5	1302.45	1.516
	119.6	1335.72	1.986
	185.4	1370.22	2.664
	238.9	1394.07	3.339
	274.1	1408.16	3.874
313.15	0.1	1216.30	1.000
	35.8	1251.96	1.259
	71.5	1281.07	1.530
	117.1	1312.56	1.916
	187.8	1351.56	2.568
	234.2	1373.59	3.039
	300.0	1400.99	3.887
323.15	0.1	1208.90	1.000
	41.8	1252.36	1.265
	84.7	1287.71	1.599
	142.7	1326.13	2.114
	212.9	1363.83	2.912
	256.4	1384.13	3.443
	330.3	1415.41	4.512

Table XI. Correlation of Shear Viscosity Data Using Free Volume Type of Equations

T (K)	V_f ($cm^3 \cdot mol^{-1}$)[a]	B_f[a]	rms % dev[a]	$V_{f'}$ ($cm^3 \cdot mol^{-1}$)[b]	$B_{f'}$[b]	rms % dev[b]
278.15	51.0	1.78	1.55	60.0	0.58	0.34
288.15	49.0	1.91	1.48	54.0	1.08	0.94
298.15	48.0	2.05	0.89	47.0	2.22	0.41
313.15	45.0	2.34	0.79	43.0	2.83	0.62
323.15	46.0	2.19	1.51	50.0	1.50	1.37

[a] Using Eq. (33).
[b] Using Eq. (35).

Equation (33) can be modified to give the effect of pressure on the viscosities of the fluids

$$\ln(\eta_p/\eta_{0.1}) + (2/3)\ln(V_p^m/V_{0.1}^m) = B_{f'}V_{f'}[1/(V_p^m - V_{f'}) - 1/(V_{0.1}^m - V_{f'})] \quad (35)$$

where V_p^m and $V_{0.1}^m$ are the molar volumes at pressures p and 0.1 MPa. The advantage of representing the viscosity ratios, using Eq. (35), is the improved fit of the data with the root mean square deviation less than that obtained using Eq. (33). The optimized values of the coefficients $B_{f'}$ and $V_{f'}$ are listed in Table XI, in which the root mean square deviations are also shown.

Many of the transport theories predict a relationship between the self-diffusion coefficient and the shear viscosity which can be expressed by the Stokes–Einstein relation

$$D\eta/T = K_1 \quad (36)$$

where K_1 is a constant depending upon the nature of the liquid but not upon the temperature and pressure. Examination of the viscosity product at constant pressure, $(D\eta/T)_p$ (Table XIIA) shows that the values decrease with temperature at constant pressure and increase with pressure at constant temperature with the exception of 313.15 K. The viscosity product at constant volume $(D\eta/T)_v$ in Table XIIB shows a similar temperature dependence to that of $(D\eta/T)_p$ at constant pressure. Examination of the values of $(D\eta/T)_v$ indicates that the values at the same temperature exhibit less variation with decrease in volume than $(D\eta/T)_p$ with increase in pressure.

One of the simplest of transport theories [66] leads to the result

$$D\eta/\rho T = \text{constant} \quad (37)$$

and the results for a wide variety of liquids can be correlated to within about $\pm 4\%$. Inspection of Table XIIB shows that the ratio is volume independent within the combined experimental uncertainty of diffusion and shear viscosity. Equation (37) correlates the data better than Eq. (36) for the temperatures 278 and 288 K.

Pollack and Enyeart [67] modified the Stokes–Einstein relation to an empirical form,

$$D\eta^q/T = K_2 \tag{38}$$

where q is between zero and one and K_2 is a constant. The same form was deduced later on the basis of assumptions on the density dependence of transport coefficients [68] and independently again on the basis of mean

Table XII. Viscosity Correlations at Various Pressures, Volumes, and Temperatures[a]

(A) Constant pressure					
	$D\eta/T$ and $(D\eta^{0.9}/T)^b$ at p				
T	0.1	50	100	150	200
288.15	4.52	4.71	4.91	5.00	5.13
	4.58	4.63	4.69	4.64	4.64
298.15	4.47	4.65	4.67	4.80	4.97
	4.57	4.62	4.51	4.53	4.63
313.15	4.47	4.21	4.07	3.88	3.85
	4.66	4.27	4.02	3.75	3.64
(B) Constant volume					
	$D\eta/T$ and $(D\eta/\rho T)^c$ at V_m				
T	77	76	75	74	73
288.15	4.66	4.76	4.86	4.97	5.07
	3.62	3.66	3.68	3.72	3.74
298.15	4.56	4.60	4.67	4.74	4.83
	3.55	3.53	3.54	3.55	3.56
313.15	4.02	4.00	4.02	3.96	4.20
	3.13	3.07	3.05	2.96	3.10

[a] Units: pressure in $10^6\ N \cdot m^{-2}$, $D\eta/T$ in $10^{-12}\ J \cdot m^{-1} \cdot K^{-1}$, ρ in $g \cdot cm^{-3}$, and V_m in $cm^3 \cdot mol^{-1}$.

[b] Second line at each temperature in A.

[c] Second line at each temperature in B.

free path theory [69]. This modified form has been tested on the diffusion and viscosity data for DCE, and for $q = 0.9$ the values of K_2 are reported in Table XIIA; the averaged result $K_2 = 4.4$ in Eq. (38) correlates the data within 9% with the exception of two data points, for 150 and 200 MPa at 313.15 K, which are approximately 20% off from K_2.

RHS theory has also been used to interpret viscosity data [54]. The basis of the application of this model to viscosity data was the Alder, Gass, and Wainwright observation [47] that within the computational uncertainty of $\pm 10\%$, the combination of the simulation results for self-diffusion and shear viscosity of the hard-sphere fluid obeyed the Stokes–Einstein equation for the hydrodynamic slip limit by the relation

$$D\eta\sigma L/RT = 0.159 \tag{38}$$

It follows from Eq. (39) that the shear viscosity of a smooth hard-sphere fluid is given by

$$\eta_{\mathrm{SHS}} = RT/2\pi L\sigma D_{\mathrm{SHS}} \tag{40}$$

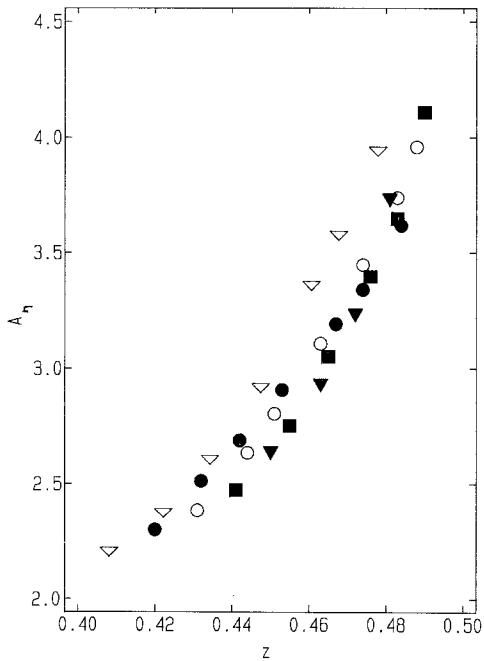

Fig. 8. Dependence of A_η factors for viscosity on packing fraction. ▼, 278 K; ■, 288 K; ○, 298 K; ●, 313 K; ▽, 323 K.

and

$$\eta = A_\eta \eta_{SHS} \tag{41}$$

The values of η_{SHS} are obtained using σ from Eq. (27) and D_{SHS} from Eq. (22). The values of A_η obtained using Eq. (41) are shown as a function of packing fraction Z in Fig. 8. The values of A_η increase with increasing temperature at constant packing fraction and increase with increased packing fraction at constant temperature. (Such behavior for A_η has been observed previously only in the case of benzene [41].) The variation of A_η for DCE with packing fraction is, as expected, opposite to that of A_D.

For hard-sphere fluids obeying the Stokes–Einstein relation [Eq. (39)] for the hydrodynamic slip limit, Harris [70] deduced that the product of the roughness factors for both diffusion A_D and viscosity A_η should be unity. For DCE, it is observed that the product of A_D and A_η [obtained from a smooth curve through A_D as a function of packing fraction (Fig. 6) and through A_η as a function of packing fraction at each temperature (Fig. 8), respectively] for packing fraction 0.43 to 0.49 varies within $\pm 9\%$ from unity.

4. CONCLUSION

Previous studies of DCE have explained temperature [2–4] and pressure effects [5, 6] on its properties by attributing them to change in the ratio of the *trans* and *gauche* forms. The closer packing geometry [71] of the molecules in the *gauche* conformation leads to a decrease in volume which has been determined as $-2.9\,cm^3 \cdot mol^{-1}$ [6]. The change from *trans* to *gauche* is accompanied by an increase in dipole moment [72].

The anomalous behavior detected in the present volumetric, diffusion, and viscosity studies especially at the higher temperatures and pressures is possibly a consequence of the varying proportion of the two molecular conformers with temperature and pressure. In particular, the deviation of reduced diffusion coefficients D^* at 313.15 K, in Fig. 7, from the curve given by Eq. (30) is also believed to be the result of the effect of temperature and pressure changing the relative proportions of the two rotational conformers. This speculation is strengthened by examining the plots for A_D in Fig. 6 and A_η in Fig. 8 as they illustrate temperature and density dependence of both parameters. The temperature-dependent variation of A_D with density is more pronounced at the higher density. An increase in temperature produces an increased proportion of *trans* rotational conformer [3, 4], whereas increasing the pressure has the opposite effect [5, 9]. The closer packing of the *gauche* conformation is likely to result in

a decreased value for the coupling factor A_D in the case of self-diffusion and a greater value for the coupling factor A_η in the case of viscosity. It is unfortunate that present data [73] for the self-diffusion of ethane are not of sufficient accuracy to enable a reliable comparison of the present results with those for ethane; this might enable determination of the conditions at which the change from *trans* → *gauche* affects the diffusion behavior.

Some evidence of the effects of the varying populations of molecular conformers is also seen in the volume and temperature dependence of the internal pressure in Fig. 4. It is possible that at 338.15 K the increased proportion of the *trans* conformation (a change from 22 to 40% *trans* accompanies a temperature increase from 253 to 303 K [4]) results in a significant decrease in dipole–dipole interactions. However, increasing pressure at constant temperature may result in a net increase in dipole–dipole interactions as a consequence of the increasing proportion of the *gauche* conformer [5]. Clearly the net result of these competing effects is difficult to estimate with the present data.

REFERENCES

1. R. J. Abraham and E. Bretschneider, *Internal Rotation in Molecules*, W. J. Orville-Thomas, ed. (Wiley, London, 1974).
2. K. Tanaka, *Spectrochim. Acta* **28**:407 (1972).
3. K. Kveseth, *Acta Chem. Scand. A* **28**:482 (1974).
4. F. J. Bermejo, E. Enciso, J. C. Dore, P. Chieux, N. Garcia, and J. Santoro, *J. Chem. Phys.* **87**:7171 (1987).
5. Y. Taniguchi, H. Takaya, P. T. T. Wong, and E. Whalley, *J. Chem. Phys.* **75**:4815 (1981).
6. S. Ikawa and E. Whalley, *J. Chem. Phys.* **81**:1620 (1984).
7. W. L. Jorgenson, R. C. Binning, Jr., and B. Bigot, *J. Am. Chem. Soc.* **103**:4393 (1981).
8. E. Enciso, J. Alonso, N. G. Almarza, and F. J. Bermejo, *J. Chem. Phys.* **90**:413 (1989).
9. E. Enciso, J. Alonso, N. G. Almarza, and F. J. Bermejo, *J. Chem. Phys.* **90**:422 (1989).
10. P. J. Back, A. J. Easteal, and L. A. Woolf, *J. Phys. E Sci Instrum.* **15**:360 (1982).
11. A. J. Easteal and L. A. Woolf, *J. Chem. Thermodyn.* **14**:755 (1982).
12. S. E. Babb, Jr., *Rev. Mod. Phys.* **35**:400 (1963).
13. J. H. Dymond, K. J. Young, and J. D. Isdale, *Int. J. Thermophys.* **1**:345 (1980).
14. A. J. Easteal, L. A. Woolf, and F. L. Wilson, *J. Mag. Reson.* **54**:158 (1983).
15. J. D. Isdale, A. J. Easteal, and L. A. Woolf, *Int. J. Thermophys.* **6**:439 (1985).
16. R. Mills and L. A. Woolf, *The Diaphragm Cell* (ANU Press, Canberra, 1968).
17. A. J. Easteal, R. Mills, and L. A. Woolf, *J. Phys. Chem.* **93**:4968 (1989).
18. M. A. McCool and L. A. Woolf, *High Temp. High Press.* **4**:85 (1972).
19. R. L. Hurle, Ph.D. thesis (Australian National University, Canberra), 1981.
20. K. R. Harris, R. Mills, P. J. Back, and D. S. Webster, *J. Mag. Reson.* **29**:473 (1978).
21. J. A. Riddick and W. B. Bunger, *Organic Solvents. Physical Properties and Methods for Purification*, 3rd ed. (Wiley–Interscience, New York, 1970).
22. A. Kumagai and S. Takahashi, *J. Chem. Thermodyn.* **17**:977 (1985).
23. W. L. Masterton and H. K. Seiler, *J. Phys. Chem.* **72**:4257 (1968).

24. S. A. Mumford and J. W. C. Phillips, *J. Chem. Soc.* 75 (1950).
25. D. M. Newitt and K. E. Weale, *J. Chem. Soc.* 3092 (1951).
26. A. T. J. Hayward, *Br. J. Appl. Phys.* **18**:965 (1967).
27. R. E. Gibson and O. H. Loeffler, *J. Am. Chem. Soc.* **63**:2287 (1941).
28. W. G. Cutler, R. H. McMickle, R. H. Webb, and R. W. Schiessler, *J. Chem. Phys.* **29**:727 (1958).
29. J. H. Dymond and R. Malhotra, *Int. J. Thermophys.* **8**:541 (1987).
30. J. H. Dymond, R. Malhotra, J. D. Isdale, and N. F. Glen, *J. Chem. Thermodyn.* **8**:603 (1988).
31. A. J. Easteal and L. A. Woolf, *Int. J. Thermophys.* **6**:331 (1985).
32. E. Wilhelm, J.-P. E. Grolier, and M. H. K. Ghassemi, *Ber. Bunsenges. Phys. Chem.* **81**:925 (1977).
33. E. Wilhelm, R. Schano, G. Becker, G. H. Findenegg, and F. Kohler, *Trans. Faraday Soc.* **65**:1443 (1969).
34. G. H. Findenegg and F. Kohler, *Trans. Faraday Soc.* **63**:870 (1967).
35. D. Tyrer, *J. Chem. Soc.* **105**:2534 (1914).
36. L. A. K. Staveley, W. I. Tupman, and K. R. Hart, *Trans. Faraday Soc.* **51**:323 (1955).
37. A. F. M. Barton, *J. Chem. Educ.* **48**:156 (1971).
38. R. E. Gibson and O. H. Loeffler, *J. Am. Chem. Soc.* **63**:898 (1941).
39. D. Chandler, *J. Chem. Phys.* **62**:1358 (1975).
40. J. H. Dymond, *Chem Soc. Rev.* **3**:317 (1985).
41. A. J. Easteal and L. A. Woolf, *Physica* **124B**:182 (1984).
42. A. J. Easteal and L. A. Woolf, *J. Chem. Soc. Faraday Trans. I* **81**:2821 (1985).
43. A. J. Easteal and L. A. Woolf, *Int. J. Thermophys.* **8**:71 (1987).
44. A. J. Easteal and L. A. Woolf, *High Temp. High Press.* **17**:271 (1985).
45. S. Meckl and M. D. Zeidler, *Mol. Phys.* **63**:85 (1988).
46. S. Chapman and T. G. Cowling, *The Mathematical Theory of Non-Uniform Gases* (Cambridge University Press, Cambridge, 1970).
47. B. J. Alder, D. M. Gass, and T. E. Wainwright, *J. Chem. Phys.* **53**:3813 (1970).
48. A. J. Easteal, L. A. Woolf, and D. L. Jolly, *Physica* **121A**:286 (1983).
49. R. J. Speedy, *Mol. Phys.* **62**:509 (1987).
50. R. J. Speedy, *Physica B* **121**:153 (1983).
51. R. J. Speedy, *Ann. N.Y. Acad. Sci.* **484**:214 (1986).
52. L. V. Woodcock, *Ann. N.Y. Acad. Sci.* **371**:274 (1981).
53. L. V. Woodcock and C. A. Angell, *Phys. Rev. Lett.* **47**:1129 (1981).
54. A. J. Easteal and L. A. Woolf, *Physica* **124B**:173 (1984).
55. J. H. Dymond, *Physica* **74**:100 (1974).
56. R. J. Hurle and L. A. Woolf, *J. Chem. Soc. Faraday Trans. I* **78**:2238 (1982).
57. R. C. Reid, J. M. Prausnitz, and B. E. Poling, *The Properties of Gases and Liquids*, 4th ed. (McGraw–Hill, New York, 1987).
58. W. M. Heston, Jr., E. J. Hennelly, and C. P. Smyth, *J. Am. Chem. Soc.* **72**:2071 (1950).
59. R. J. Fort and W. R. Moore, *Trans. Faraday Soc.* **62**:1112 (1965).
60. E. J. Bair and C. A. Kraus, *J. Am. Chem. Soc.* **73**:2459 (1951).
61. J. J. Zwolenik and R. M. Fuoss, *J. Phys. Chem.* **68**:903 (1964).
62. J. H. Dymond and T. A. Brawn, in *Proc. 7th Symp. Thermophys. Prop.*, A. Cezairliyan, ed. (Am. Soc. Mech. Eng., New York, 1977), p. 660.
63. J. H. Dymond, J. Robertson, and J. D. Isdale, *Int. J. Thermophys.* **2**:133 (1981).
64. J. H. Dymond and K. J. Young, *Int. J. Thermophys.* **2**:237 (1981).
65. H. Kashiwagi and T. Makita, *Int. J. Thermophys.* **3**:289 (1982).
66. C. J. Vadovic and C. P. Colver, *A. I. Chem. Eng. J.* **18**:1264 (1972).

67. G. L. Polack and J. H. Enyeart, *Phys. Rev. A* **31**:980 (1985).
68. R. Zwanzig and A. K. Harrison, *J. Chem. Phys.* **83**:5861 (1985).
69. B. C. Eu, *J. Chem. Phys.* **89**:485 (1988).
70. K. R. Harris, *Physica* **93A**:593 (1978).
71. M. Aroney, D. Izsak, and R. J. W. Le Fevre, *J. Chem. Soc.* 1407 (1962).
72. D. Chandler, *Discuss. Faraday Soc.* **66**:184 (1978).
73. C. G. Wade and J. S. Waugh, *J. Chem. Phys.* **43**:3555 (1965).